Using Solid Mechanics to Evaluate the Capillary and Viscous Behavior of Noncircular Tube Shapes

Robert W. Cornell; Lexmark International, Inc; Lexington, KY/USA

Abstract

The similarity between torsion-solid mechanics and incompressible-viscous tube flow is investigated by finite element solutions of the governing partial differential equations. After the numerical solutions are validated against several well-known analytical functions for noncircular shapes, a method is presented to illustrate how hydraulic resistance factors may be computed from the polar moment of inertia. Since the results are scaleable, the macroscopic solid mechanics information can be used to predict the viscous pressure loss term for micro-machined flow features. The numerical technique is then further developed to estimate the Laplace pressure jump across the main terminal meniscus in noncircular capillaries. The solid mechanics based numerical technique is demonstrated on several special cases involving horizontal and vertical capillary flow in noncircular regimes. The numerical technique compares well to published experimental results. Then a nozzle shape figure of merit is derived, and applied to a variety of noncircular shapes. Finally, the numerical methods are merged into the LXK droplet simulation model where their effectiveness is demonstrated against lab data from a wide experimental space for thermal inkjet.

Introduction

Fluid flow in micro-machined channels is a central topic in the inkjet industry. It finds broad applications in other MEMS devices as well. Analytical methods exist to compute the viscous and capillary behavior of simple shapes; like elliptical, rectangular and triangular tube shapes. For more complex shapes, the hydraulic diameter approximation is often used, but it is well-known that this method produces large errors. It will be shown that a numerical technique used for analyzing torsion in solid metal bars leads to a method for quantifying the viscous and capillary behavior of noncircular tubes. A method is then presented showing how to experimentally determine the micro-scale viscous and capillary behavior of noncircular tubes from a macro-scale solid mechanics test.

Since refill time is a fundamental parameter limiting the fire frequency of thermal inkjet, it is desirable to investigate; what is the optimum nozzle shape? To that end, a dimensionless, nozzle shape figure of merit is derived and exercised on a variety of contenders.

Torsion of Noncircular Bars

When torque is applied to a noncircular bar, the displacements have horizontal and vertical components. It can be shown that the governing equation is [1]:

$$\frac{\partial^2\Phi}{\partial x^2}+\frac{\partial^2\Phi}{\partial y^2}+2G\Theta=0 \qquad (1)$$

Φ = warping function
$\Phi(\Gamma) = 0$ on the boundary
G = shear modulus of the material (Pa)
Θ = twist angle per unit length (rad/m)

Across any (x, y) cross section, the warping function represents a surface. Torque is proportional to the volume under this surface, and shear stress is proportional to the gradients of Φ.

$$T = 2\int_{Area}\Phi dA \qquad (2)$$

$$\tau_{zx}=\frac{\partial\Phi}{\partial x};\tau_{zy}=\frac{\partial\Phi}{\partial y} \qquad (3)$$

T = torque (N-m)
τ_{ij} = shear stress components (Pa)

Note that Eq.(1) has the same form as the Navier-Stokes equation for one dimensional, viscous, incompressible flow. Also note that Eq.(2) has a form similar to the expression for volumetric flow rate, and Eq.(3) has a form similar to the shear stress term for Newtonian fluids. The similarity even applies to the boundary conditions. In the torsion problem Φ goes to zero on the boundary, and in the tube flow analog, velocity goes to zero at the wall.

Incompressible Viscous Tube Flow

For low Reynolds numbers, as is typical in capillary flow, it is reasonable to assume that the liquid velocity has only one component, (u) along the tube axis. The Navier-Stokes equation reduces to [2]:

$$\frac{\partial^2 u}{\partial x^2}+\frac{\partial^2 u}{\partial y^2}-\frac{1}{\mu}\frac{dp}{dz}=0 \qquad (4)$$

μ = dynamic viscosity (Pa-s)
u = axial velocity (m/s)
$u(\Gamma) = 0$ at the wall
dp/dz = pressure gradient in the flow direction (Pa/m)

The flow analog of torque is volumetric flow rate dV/dt (m^3/s):

$$\frac{dV}{dt}=\int_{Area}u(t)dA \qquad (5)$$

The similarity between Eq.(1,4) and Eq.(2,5) is readily apparent. This suggests that the finite element analysis techniques [3] used to solve the solid mechanics problem may also be used for the viscous tube flow problem, but before illustrating that let us define the flow resistance factor (β).

$$\beta = \frac{dp/dz}{\mu Q} \tag{6}$$

β = flow resistance factor (m^{-4})
dp/dz = pressure gradient (Pa/m)
μ = dynamic viscosity (Pa-s)
$Q = dV/dt$ = volumetric flow rate (m^3/s)

Note that (β) has units of $length^{-4}$. Thus the flow resistance factor is purely a geometric property of the tube shape. Also, the polar moment of inertia used in solid mechanics torsion has units of ($length^4$), so the similarity continues.

Since the pressure gradient and viscosity terms are factored out in the calculation of (β), they may be set to unity. This simplifies the finite element problem to meshing just the flow cross section and solving an elliptic partial differential equation. Then the hydraulic resistance factor is obtained by integrating the solution over the tube exit area:

$$\frac{\partial^2 u^*}{\partial x^2} + \frac{\partial^2 u^*}{\partial y^2} = 1 \tag{7}$$

$$\beta = \frac{1}{\int_{Area} u^* dA} \tag{8}$$

$u^*(x,y)$ = velocity function
$u^*(\Gamma) = 0$: the velocity function goes to zero at the wall
β = hydraulic resistance factor (m^{-4})

Now let's illustrate the similarity of solutions between solid mechanics (Φ) and the velocity function (u^*). Let's assume the cross section is the interstitial cavity formed by three 1 mm rods, and a similarly shaped torsion bar. Figure 1 shows the finite element solution for the velocity function (u^*), and Figure 2 shows the normalized warping function (Φ) for the solid torsion bar. The solutions are identical.

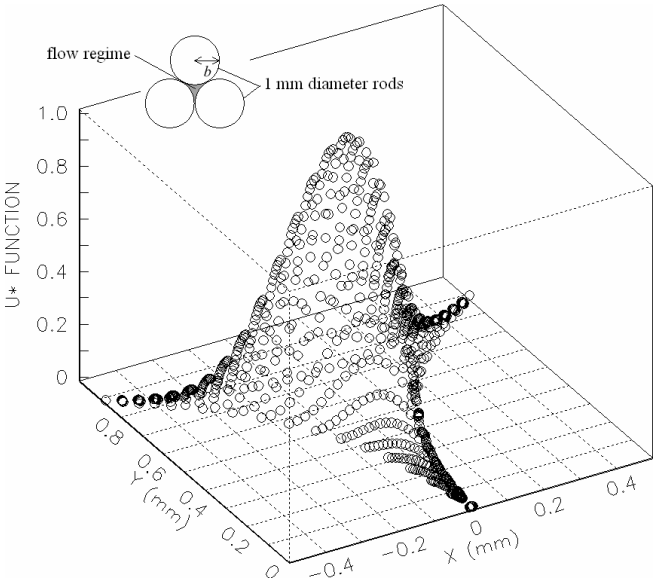

Figure 1: *Velocity function (u*) for flow regime of triangular packed rods*

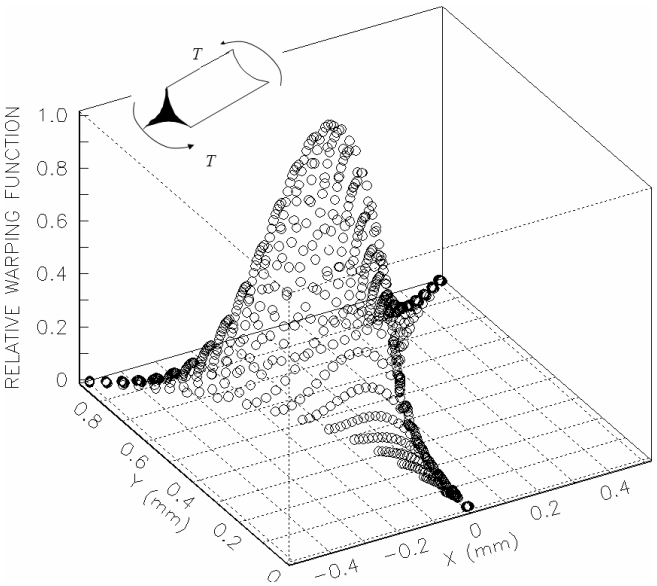

Figure 2: *Warping function (Φ) for similar shaped torsion bar*

Hydraulic Resistance Factor

For noncircular tubes, the problem has long been how to use Poiseulle's equation [Eq.(9-10)] when the tube cross section cannot be defined simply by a diameter (d). The hydraulic approximation method is found as frequently in the literature as are references to the large errors that it produces for noncircular cross sections. Inserting Eq.(12) into Eq.(11) is supposed to provide an estimate of the hydraulic resistance factor [5].

$$\Delta P_1 = \beta \mu L \frac{dV}{dt} \tag{9}$$

$$\beta = \frac{128}{\pi d^4} \quad \text{for circular tubes} \tag{10}$$

$$\beta = \frac{128}{\pi D_{HYD}^{\ 4}} \quad \text{for noncircular tubes} \tag{11}$$

$$D_{HYD} \approx 4 \frac{\text{tube cross section area}}{\text{wetted perimeter}} = \text{Hydraulic approximation} \tag{12}$$

ΔP_1 = pressure drop due to flow in the tube (Pa) [4]
L = tube length (m)
$dV/dt = Q$ = volumetric flow rate (m^3/s)
d = tube diameter (m)
β = hydraulic resistance factor for the tube (m^{-4})
D_{HYD} = hydraulic diameter (m)

To illustrate the folly of relying on the hydraulic approximation Eq.(12) let's use it to compute (β) for elliptical and rectangular tubes. Analytical solutions [6,7] exist [Eq.(13-15)] for both of these shapes, so we can quantify the error associated with Eq.(12). Contrasting the inaccuracy of Eq.(12), the finite element solutions of Eq.(7-8) follow the analytical solutions precisely, as shown in Figure 3.

$$\beta = \frac{12}{a^3 b}\left[1 - \frac{192a}{\pi^5 b}\sum_{i=1,3,5}^{\infty}\frac{\tanh\left(\frac{i\pi b}{2a}\right)}{i^5}\right]^{-1} \quad \text{rectangle (a}\times\text{b)} \qquad (13)$$

$$\beta = \frac{4(K+1)\sqrt{K}}{\pi a^4} \quad \text{ellipse (a}\times\text{b)} \qquad (14)$$

$$K = \left(\frac{a}{b}\right)^2 \qquad (15)$$

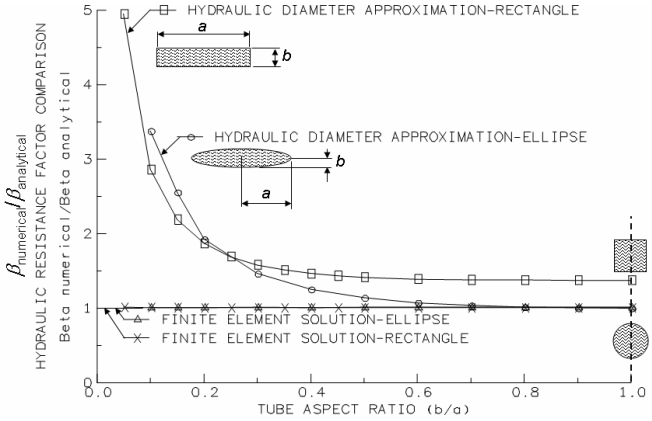

Figure 3: *Hydraulic approximation versus finite element solution for (β)*

Solid Mechanics and Hydraulic Resistance

An experimental practice for characterizing fluid flow in MEMS devices is the use of micro-particle image velocimetry (micro-PIV) [8]. However, as the flow channel decreases in size, so must the seed particle size. As seed particles become smaller, the effects of Brownian motion must be accounted for to obtain accurate measurements from particle tracking. In addition to this complication micro-PIV requires illumination of the flow field. MEMS and inkjet applications need an alternative method to characterize the viscous and capillary behavior of micron-scale tube flow.

As was demonstrated, the same finite element method may be used for tube flow and torsion problems because of the similarity in their governing equations. Pressure gradient drives flow, while twist angle drives torque. Shear modulus is the material property in the solid mechanics problem, while viscosity is the material property in the fluid mechanics problem. Polar moment of inertia is the geometric property of the cross section in the solid mechanics problem, and the hydraulic resistance factor is the matching parameter in the tube flow problem. All of this suggests that hydraulic resistance factors could be obtained experimentally with a mechanical test.

Flow rates may be readily measured in macroscopic flow regimes; however, micro-machined features are difficult to characterize experimentally. This is where the solid mechanics approach can help. The following procedure permits a relatively simple torsion test to be translated such that it reveals information about the flow characteristics in micro-machined features.

When the tube deviates from round, exact solutions for (β) are rare. The same is true in solid mechanics. When a torsion bar shape deviates from round, exact solutions for the polar moment of inertia (J) are rare; however, they are readily measured because the shear modulus of common metals is well known. Applying a specific twist angle per unit length (Θ) and measuring torque (T) on a metal bar with a known shear modulus (G) leads to a solution of Eq.(16) for polar moment of inertia (J).

$$T = \Theta GJ = Torque \qquad (16)$$

It can be shown that the polar moment of inertia (J) is related to the hydraulic resistance factor (β) by Eq.(17). Note that the *4*-coefficient in Eq.(17) comes from the product of the *2*-coefficients in Eq.(1-2). The inverse relationship between (J) and (β) is obvious from Eq.(6 and 16).

$$\beta = \frac{4}{J} \qquad (17)$$

The special case of round tube versus round bar provides a convenient sanity test for Eq.(17). The hydraulic resistance factor of a round tube is given by: [$\beta = 128/\pi d^4$]. The polar moment of a round bar is: [$J = \pi d^4/32$]. Combining these two expressions leads back to Eq.(17).

Thus, by the use of Eq.(17), the hydraulic resistance factor of any arbitrary tube shape may be determined by a solid mechanics torsion test on a bar of the same shape. However, MEMS flow features are on the order of microns in size, so it would be impractical to attempt a mechanical measurement of polar moment of inertia on micron size torsion bars. Fortunately, the results are scaleable. For example, to convert from a macroscopic, centimeter scale solid torsion bar to a micron sized MEMS flow tube, the appropriate scale factor (SF) is 10^{16} $\mu m^4/cm^4$. Thus to convert a macro-scale torsion result to a micro-scale hydraulic flow resistance factor:

$$\beta = 4\frac{SF}{J} = \text{Solid mechanics - Fluid mechanics conversion} \qquad (18)$$

For example, Kim and Whitesides [9] reported experimental data for flow in a 1.75 micron square tube. To monitor the flow they used micro-imaging to observe imbibition rate. They commented that their hydraulic diameter approximation [i.e. Eq.(12)] did not agree well with their data. Their actual flow data suggested an effective D_{HYD} value of 2.0 microns instead of the value computed by Eq.(12). What if, instead of using the hydraulic approximation method and measuring meniscus motion, they had torsion tested a 1.75 cm square, solid aluminum bar (G = 26 GPa) to predict the actual hydraulic resistance of a 1.75 micron square tube?
Analytical expression for torsion in rectangular bars [1]:

$$Torque = T = \left(\frac{a^3 b}{K_1}\right)G\Theta : \quad (a\times b)\ \text{rectangular bar} \qquad (19)$$

$$K_1 = \left[\frac{1}{3} - \frac{64a}{\pi^5 b}\sum_{n=0}^{\infty}\frac{\tanh\left(\frac{(2n+1)\pi b}{2a}\right)}{(2n+1)^5}\right]^{-1} \qquad (20)$$

- By Eq.(19-20), or by finite element analysis of Eq.(1-2), or by mechanical measurement: $J = 1.311 \times 10^{-8}$ m^4
- By Eq.(18): $\beta = 3.051 \times 10^{24}$ m^{-4}

- Then by Eq.(11): D_{HYD} = 1.95 microns. This compares quite well with the 2 μm value suggested by Kim & Whitesides' data

Therefore, a simple, macroscopic torsion test on a 1.75 cm solid aluminum bar would have given the Harvard researchers the microscopic flow characteristic they were seeking.

Capillary Flow

When liquid penetrates a capillary, the meniscus at the base of the liquid-gas interface is often referred to as the main terminal meniscus. The curvature of the main terminal meniscus dictates its capillary rise. Capillary rise in vertical tubes may be computed by equating the Laplace pressure jump across the meniscus to the gravimetric pressure head. Capillary rise (h) is defined by the well-known [10]:

$$h = \left(\frac{2\kappa\sigma}{\rho g} \right) \tag{21}$$

Where:
h = meniscus rise (m)
σ = surface tension of the liquid (N/m)
ρ = liquid density (kg/m^3)
g = acceleration due to gravity (m/s^2)
κ = meniscus curvature (m^{-1})

For circular tubes the solution to Eq.(21) is straightforward because meniscus curvature (κ) is simply ($2\cos\theta/d$), where θ is the tube wall-meniscus contact angle, and d is the tube diameter. For noncircular tubes the solution to Eq.(21) is not straightforward because meniscus curvature is generally unknown. To sidestep this difficulty it is common practice to substitute the hydraulic diameter approximation (D_{HYD}) of Eq.(12) into Eq.(21) in place of (d). However, it was demonstrated in Figure 3 that D_{HYD} provides an inaccurate estimator for computing (β), so there should be little hope that it will be an accurate estimator of capillary rise in noncircular tubes. Rather than use the wetted perimeter approximation, let us approach the problem a little differently. The finite element solution of Eq.(7-8) provided accurate results for the hydraulic resistance factor (β), as did the solid mechanics torsion test method described by Eq.(18). Rearranging Eq.(21) such that capillary rise (h) is a function of the hydraulic resistance factor (β):

$$h = \left(\frac{2\sigma\cos\theta}{\rho g} \right) \left(\frac{8}{\pi\beta} \right)^{-1/4} \tag{22}$$

Now let us validate this expression against a variety of special cases that have known experimental results.

Capillary Rise Model Validation

Experimental data for several noncircular cases has been reported by Bico and Quere'[11]. They measured the vertical rise of the main terminal meniscus of cyclohexane in perfectly wetting square tubes. Figure 4 verifies that the measured data is well represented by the solution methods presented in this paper. The same authors also published data for capillary rise in fiber bundles. Recall that Figure 1 showed the velocity function for the triangular packing case. Figure 5 verifies that the model described here well-represents that experimental data too.

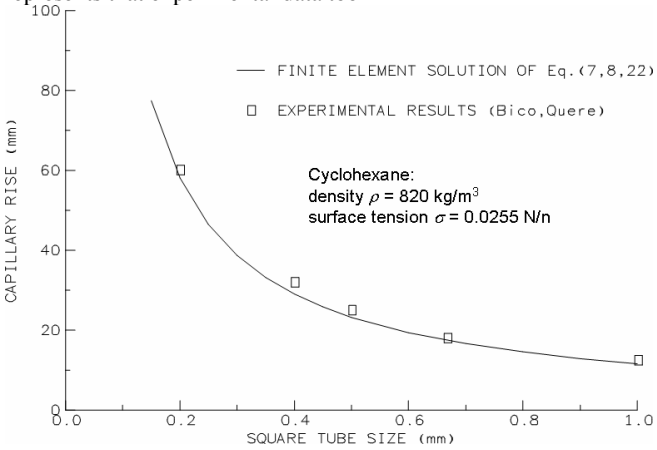

Figure 4: *Capillary rise of cyclohexane in square tubes*

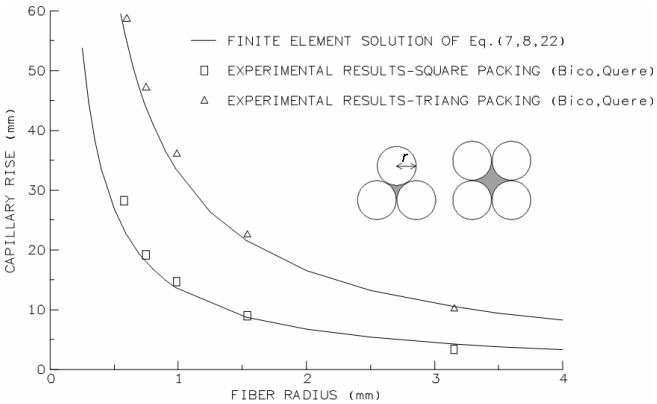

Figure 5: *Capillary rise of cyclohexane in fiber bundles*

An especially interesting capillary is formed by a rod-in-corner. Figure 6 illustrates the velocity function for this special case. The (β) values derived from this flow field are then used in Eq.(22) to compute capillary rise. Experimental results have been reported by Mason and Morrow [12] for the rod-in-corner capillary. Their experiment placed perfectly wetting steel rods against the corner of an L-shaped aluminum slab. Their measured iso-octane rise is compared against the numerical solutions of this paper in Figure 7. Once again the results are remarkably consistent.

It is important to note at this point that the earlier described torsion test method could also have been used because we now know that it is possible to transform a solid mechanics experiment into a fluid mechanics (β) value by use of Eq.(18), and then use Eq.(22) to compute capillary rise (h).

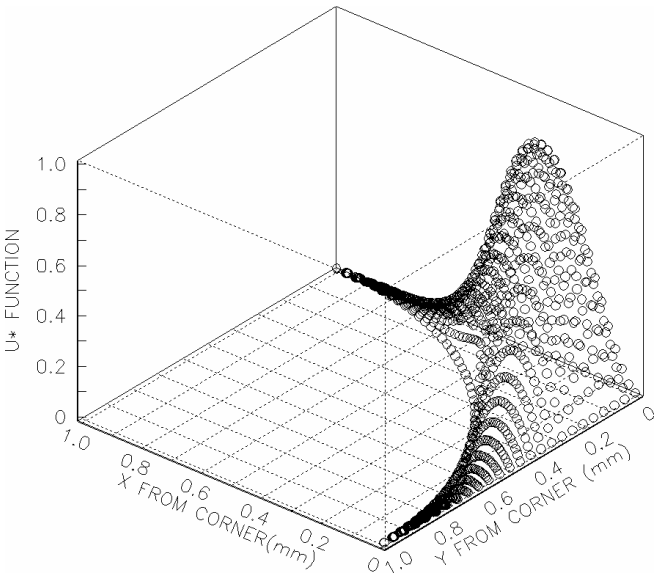

Figure 6: *Velocity function for rod-in-corner capillary*

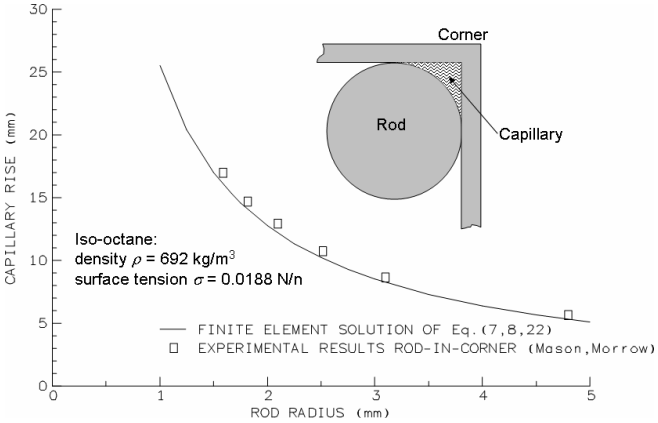

Figure 7: *Rise of iso-octane for rod-in-corner capillary*

Horizontal Capillary

When the capillary tube is horizontal, the gravimetric pressure goes to zero, so Eq.(22) does not apply. Nor does it apply in cases where the Bond number is <<1 (e.g. MEMS, inkjet). For cases where the gravitational effect is negligible, the Washburn equation [10] Eq.(23) relates the Laplace pressure jump across the meniscus to the viscous pressure drop due to flow.

$$z' = \frac{\sigma \cos\theta}{4\mu L} r \tag{23}$$

Where:
z' = imbibition front velocity (m/s)
r = capillary tube radius (m)
L = length of liquid imbibition front (m)
(σ,θ,μ) previously defined

Note that Eq.(23) only applies to the special case of circular capillary shapes. When the capillary is noncircular it is common practice to estimate (r) by the wetted perimeter, hydraulic approximation method. Unfortunately, as discussed earlier, this leads to large errors as the capillary shape departs further and further from circularity.

Since it was just demonstrated that the finite element method solution of Eq.(7,8,22), or the solid mechanics torsion test method in conjunction with Eq.(18), provided very accurate results for vertical capillaries, we have every reason to expect that they will also work well on horizontal capillaries. So let us now derive an expression for imbibition velocity in a noncircular capillary with a negligible Bond number.

$$\Delta P_2 = \frac{2\sigma\cos\theta}{r} \approx \frac{2\sigma\cos\theta}{\left(\frac{8}{\pi\beta}\right)^{0.25}} \tag{24}$$

$$Q = z' \times A_T \tag{25}$$

ΔP_2 = pressure jump across the meniscus (Pa)
A_T = cross section area of the capillary (m^2)
z' = imbibition front velocity (m/s), i.e. meniscus motion
Q = volumetric flow rate (m^3/s)
σ=surface tension (N/m)
θ= contact angle (rad)
β= hydraulic resistance factor (m^{-4})
L = length of the imbibition front (m)
Setting $\Delta P_2 = \Delta P_1$, substituting Eq.(25) for Q and solving for z' we arrive at a general expression for imbibition velocity:

$$z' = \left(\frac{2\sigma\cos\theta}{\mu L A_T}\right)\left(\frac{8}{\pi}\right)^{-1/4} \beta^{-3/4} \tag{26}$$

For noncircular capillaries, (β) is solved as previously described – either by finite element analysis methods, or solid mechanics measurements of (J) the polar moment of inertia of an equivalent torsion bar. Note that for circular capillaries, Eq.(26) reverts to the Washburn equation. Also note that Eq.(26) implies a linear relationship between imbibition velocity and the interfacial free energy term ($\sigma\cos\theta$). An experimental verification of this fact exists in the earlier mentioned experiment by Kim and Whitesides [9]. They varied contact angle by chemical means and measured imbibition rate in horizontal, 1.75 μm square capillary tubes. The plot of z' versus $\cos\theta$ showed a linear relationship indeed exists. Furthermore, they reported that the slope of the regression plot corresponded to a hydraulic diameter of 2 μm. This experimental value is just 2.5% different from the number computed earlier in this paper using the solid mechanics method.

Nozzle Shape Figure of Merit

Now that we have demonstrated and validated a numerical technique to quantify the viscous and capillary behavior of any arbitrary tube shape, let's utilize it on some noncircular tubes with feature sizes in the realm of typical inkjet nozzles. Specifically, we're interested in finding the optimum nozzle shape.

The first example is a serrated capillary. This tube shape may be defined by three parameters: inside radius (b), outside radius (a) and number of teeth (N). Figure 8 shows the finite element solution of the velocity function (u^*) for a 24 tooth serrated nozzle having an inside radius of 6 μm and an outside radius of 10 μm. For this specific case, the finite element solution of Eq.(7,8) tells us that the hydraulic resistance value (β) equals 1.64×10^{21} m^{-4}, and

the exit area is 188 μm^2. Let's further assume a 20 degree contact angle and the liquid in the nozzle has inkjet-like properties (σ = 0.030 N/m). Then by Eq.(24) the meniscus pressure is 8982 Pa. A round nozzle with the same exit area would have a radius of 7.73 μm. The same liquid in an equal area round tube would have a capillary pressure of 7294 Pa. Thus for an equivalent flow area, the serrated nozzle achieves a 23% greater pressure jump across the meniscus.

Since refill is accomplished by capillary pressure, and the serrated nozzle has higher meniscus pressure than an equivalent area round nozzle, one might jump to the conclusion that inkjet nozzles should be serrated. Furthermore, it can be shown that all noncircular nozzles have higher meniscus pressure than equal area round nozzles. Indeed the literature has many examples that cite this superiority [13-17]. Given the higher meniscus pressure in noncircular nozzles, and the ever increasing speed requirements for inkjet, it begs the question*:"Why, after more than two decades of commercial products, are virtually all thermal inkjet nozzles round, or nearly round"?* Commercial inkjet products may have nozzles that are tapered along their length axis, but their cross sections are almost always circular. There must be more to the nozzle figure of merit than meniscus pressure (or meniscus curvature).

Since refill time is the gating factor with regards to inkjet fire frequency, perhaps it is appropriate to derive a nozzle figure of merit that deals with time. Consider that equal area tubes will have equal volume per unit length, and refill time is a function of replacing the volume that was just displaced by the vapor bubble. So the race to refill equal volume displacements through nozzles having equal areas will go to the nozzle shape having the highest imbibition front velocity.

Comparing the imbibition front velocity between noncircular and circular tubes of equal area with the same liquid and interface properties results in a dimensionless figure of merit for any given cross section shape. It will be shown that this figure of merit is strictly a function of cross section geometry since all other terms cancel when the ratio is formed.

$$\xi = \frac{z'_{NC}}{z'_C} \tag{27}$$

ξ = nozzle shape figure of merit
z'_{NC} = imbibition front velocity for noncircular nozzle
z'_C = imbibition front velocity for circular nozzle
Substituting Eq.(26) into Eq.(27):

$$\xi = \left(\frac{\beta_{NC}}{\beta_C}\right)^{-3/4} \tag{28}$$

β_{NC} = hydraulic resistance factor for noncircular nozzle
β_C = hydraulic resistance factor for circular nozzle
Note that (β_{NC}) is obtained by:

- Finite element solution of Eq.(7,8) – or,
- Solid mechanics torsion test and Eq.(18) to convert polar moment of inertia (J) into (β_{NC}).

Recall that for a circular capillary:

$$\beta_C = \left(\frac{128}{\pi d^4}\right) \tag{10}$$

Since we are comparing equal area nozzles (A_T), we can substitute:

$$16\left(\frac{A_T}{\pi}\right)^2 = d^4$$

So:

$$\beta_C = \left(\frac{8\pi}{A_T^{\ 2}}\right)$$

Then:

$$\xi = \left(\frac{8\pi}{\beta_{NC} A_T^{\ 2}}\right)^{3/4} = \text{Nozzle shape figure of merit} \tag{29}$$

Recall that the serrated tube example had a hydraulic resistance factor of 1.64 x 10^{21} m^{-4} and a cross section area of 188 μm^2. This nozzle area might be utilized in a modern 4-7 pl droplet ejector, if indeed it proves superior to a simple circle.

Unfortunately, upon inserting these values into Eq.(29) we find that the serrated nozzle has a figure of merit (ξ) equal to 0.53. In other words, even though the serrated nozzle has a greater meniscus pressure than an equal area round tube, it also has higher viscous losses. The increased viscous loss more than offsets the meniscus pressure gain. Accordingly, it follows that an equal volume of liquid would take 53% more time to travel an equal distance in this particular serrated nozzle as it would in an equal area round nozzle.

Similar calculations on a variety of other noncircular shapes (star, elliptical and clover shaped) return (ξ) values less than unity as well. Figure 9 summarizes the figure of merit values for several nozzle shapes as a function of (b/a). Note that (ξ) goes to one as (b/a) goes to unity because at this point the cross section is a circle.

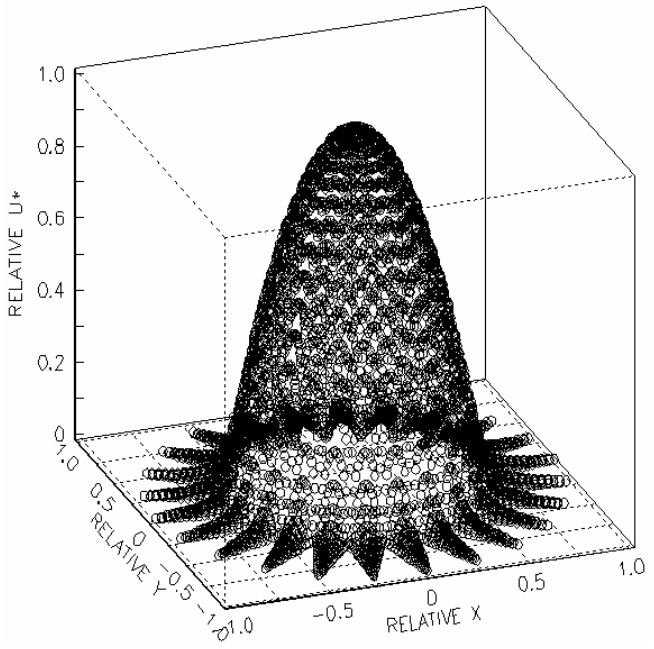

Figure 8: *Velocity function for serrated nozzle shape*

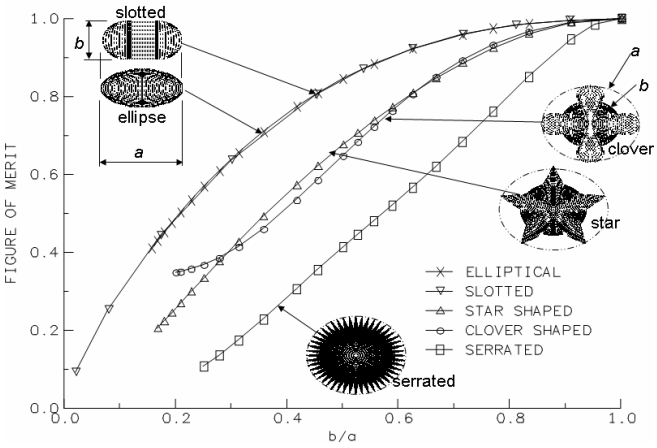

Figure 9: *Nozzle shape figure of merit*

According to Figure 9, the worst nozzle shape to use in inkjet applications would be serrated. Perhaps that is why such shapes have not made an appearance in the commercial world. Star and clover shaped nozzles do not fare much better. None of these shapes have ever shown up in a commercial product. In light of Figure 9 this fact is not surprising. Elliptical or near-elliptical slot shaped nozzles have made their way into the marketplace. These shapes are of interest for several reasons.

- As vertical resolution increases, the chip real estate available to place nozzles becomes ever smaller. An ellipse/slot permits the use of the horizontal dimension to obtain the nozzle area needed.
- Figure 9 shows that there is not much (ξ) degradation until the *b/a* ratio of an ellipse/slot shaped nozzle ratio drops below 0.5

FEAJET Simulation Model

The teachings of this article have been merged into the Lexmark inkjet simulation model (FEAJET). This model is an application-specific, multi-physics, finite element simulation tool. It accurately accounts for the electro-thermo-hydrodynamics of the inkjet printing process [18-20]. The model inputs include:

- Thin film structure
- Thin film material properties
- Resistor shape and size
- Ink formulation
- Electrical driving means
- Flow features

A representative output summary is shown in Figure 10. The tapered elliptical nozzle of Figure 10 varies in cross section over its length. This is handled by writing Eq.(9) as an integral.

$$\Delta P_1 \approx \frac{dV}{dt}\int_{x=0}^{L} \beta\mu dx \qquad (30)$$

Since inkjet flow is impulsive, the model needs more than just the flow resistance terms. It also needs to account for the inertial terms. Inertance is handled by a finite element solution of the flow potential (Ψ) over the domain.

$$\nabla^2\Psi = 0 \qquad (31)$$

$$A_i = \frac{\rho}{\oint \nabla\Psi \bullet \vec{n}_i dS} \qquad (32)$$

$$A_i \frac{d^2V_i}{dt^2} = P_v - \sum \Delta P \qquad (33)$$

Ψ = flow potential (dimensionless)
A_i = acoustic inertance at inlets, outlets *i,j,k,*…(kg/m^4)
ρ = liquid density (kg/m^3)
$\boldsymbol{n}_i$ = unit normal vector at surfaces of interest *i,j,k*…
$\boldsymbol{n}_i dS$ = area of surfaces of interest *i,j,k*…(m^2)
V_i = displaced volume at surfaces *i,j,k*…(m^3)
t = time (s)
P_V = phase change pressure at the bubble wall (Pa)
ΔP = viscous pressure drop (Pa)

Eq.(33) is analogous to transient current flow in a parallel path *LR* circuit. There is insufficient space here to describe the FEAJET solution means for the other variables in the simulation:

- 2D Electric field (by finite element)
- 2D Current density field (by finite element)
- 2D Transient heat transfer (by finite element)
- Ink formulation dependent nucleation response
- Viscosity-temperature-evaporation response of the mixture
- Thermodynamic properties of the mixture
- Liquid-vapor phase change
- Bubble growth and collapse
- Refill time and meniscus dynamics

The simulation-experimental correlation for the ejector of Figure 10 is excellent:

- Simulated droplet volume 27.3 vs. 27 pl measured
- Simulated droplet velocity 508 vs. 524 in/s measured
- Simulated refill time 104 vs. 100 μs measured

Figures 11-12 show the correlation between simulation and experimental results over a wide experimental space.

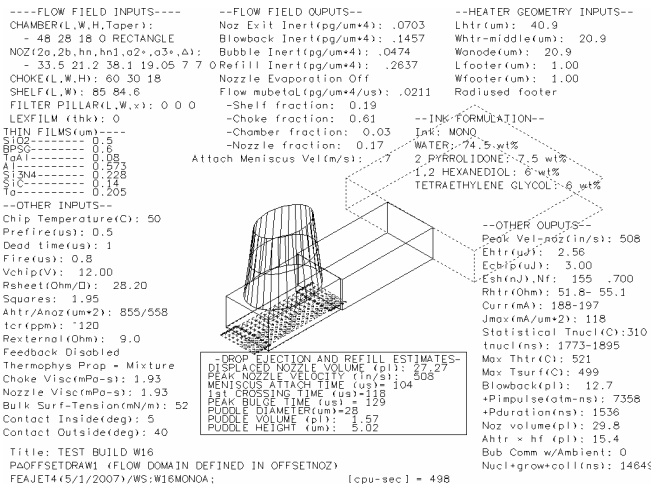

Figure 10: *Typical FEAJET simulation result*

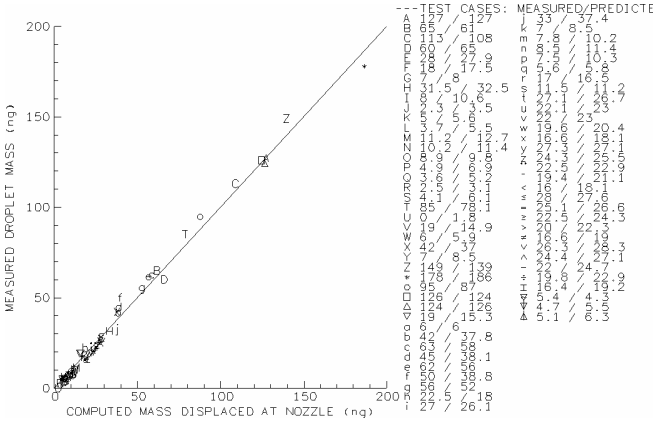

Figure 11: *Droplet mass correlation: simulation vs. measured*

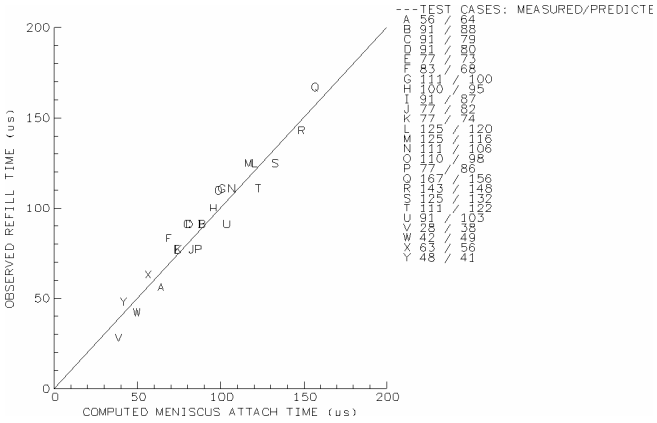

Figure 12: *Refill time correlation: simulation vs. measured*

Summary

Because of the similarities in their governing equations, laminar-viscous-incompressible flow in noncircular tubes may be solved with the same numerical techniques as used in torsion, solid mechanics problems. The method was then expanded to include capillary effects. The numerical technique was validated against known analytical solutions and published experimental data. A method of translating macroscopic torsion test results into hydraulic resistance factors and meniscus curvature values was also presented.

A nozzle figure of merit was derived. The figure of merit was based upon the imbibition front velocity in capillaries with negligible Bond numbers. It showed that the preferred inkjet nozzle cross section is circular because the race to refill equal volumes of liquid, in equal area nozzles, will go to the circular shape not the noncircular shape. In cases where chip real estate is limited (i.e. closely spaced, high dpi ejectors) ellipse/slot shaped nozzles may be used as long as the minor/major dimension is greater than 0.5.

Finally, the numerical techniques were merged with the Lexmark electro-thermo-hydrodynamic simulation tool. The correlation between lab data and numerical results has been excellent over a wide experimental space.

References

[1] F.A. D'Isa, Mechanics of Metals, (Addison-Wesley, Reading, PA, 1968), pg. 94-104.

[2] G.K. Batchelor, An Introduction to Fluid Dynamics, (Cambridge Univ. Press, Cambridge, G.B., 1967), pg. 182.

[3] L.J. Segerlind, Applied Finite Element Analysis, (Wiley & Sons, New York, NY, 1984), pg. 100-110.

[4] I.H. Shames, Mechanics of Fluids, (McGraw-Hill, New York, NY, 1962), pg. 298.

[5] F. Kreith & M.S. Bohn, Principles of Heat Transfer, (Harper & Row, New York, NY, 1986), pg. 287.

[6] R.L. Panton, Incompressible Flow, (Wiley & Sons, New York, NY, 1995), pg. 263-266.

[7] M. Dong & I. Chatzis, J. Colloid Interface Sci., 172, 278, (1995).

[8] S. Wereley, C.D. Meinhart, S. Stone, V. Hohreiter, J. Chung, J. Proc. SPIE, 4558, 124, (2001).

[9] E. Kim & G.M. Whitesides, J. Phys. Chem., 101, 855, (1997).

[10] E.W. Washburn, Phys. Rev., 47, 273, (1921).

[11] J. Bico & D.M. Quere', J. Colloid Interface Sci., 247, 162, (2002).

[12] G. Mason & N.R. Morrow, J. Chem. Soc. Faraday Trans 1, 80, 2375, (1984).

[13] C.S. Chan & G.E. Hanson, US 4791436, (1987).

[14] R.C. Maze, T.L. Weber & A.K. Agarwal, US 6371596, (1999).

[15] M. Tachihara, Y. Tamura & S. Murakami, US 6350016, (1999).

[16] T.L. Weber, EP 0 770 487, (1996).

[17] P. McGuiness, W. Drenkhan & D. Weaire, J. Phys. D: Appl. Phys., 38, (2005).

[18] R.W. Cornell, P. IS&T NIP14, pg. 9-14 (1998).

[19] R.W. Cornell, P. IS&T NIP16, pg. 21-27, (2000).

[20] R.W. Cornell, Recent Progress in Ink Jet Technologies II, (IS&T Springfield, VA, 1999), pg. 108-113.

Author Biography

Robert Cornell is a Senior Technical Staff Member in Lexmark's R&D Organization. He is the developer of FEAJET, Lexmark's droplet simulation model that includes phase change, and the electro-thermo-hydrodynamics of bubble nucleation, growth and droplet ejection. He has authored 4 previous papers for IS&T, and he holds 29 US patents. Over the last 30 years he has been involved in a wide range of inkjet and impact printer programs at Lexmark and IBM. He is a member of IS&T.